Flow separation control by dielectric barrier discharge plasma actuation via pulsed momentum injection

Cite as: AIP Advances **8**, 075229 (2018); https://doi.org/10.1063/1.5037770
Submitted: 27 April 2018 • Accepted: 18 July 2018 • Published Online: 30 July 2018

Julie A. Vernet, Ramis Örlü and P. Henrik Alfredsson

Flow separation control by dielectric barrier discharge plasma actuation via pulsed momentum injection

Julie A. Vernet,[a] Ramis Örlü,[b] and P. Henrik Alfredsson[c]
Linné FLOW Centre, KTH Mechanics, SE-100 44 Stockholm, Sweden

(Received 27 April 2018; accepted 18 July 2018; published online 30 July 2018)

Control of a turbulent boundary layer separating on a half-cylinder mounted on a flat plate has been investigated using a Dielectric Barrier Discharge (DBD) plasma actuator placed along the apex of a cylinder. The main focus of the study has been to evaluate if the control ability of the actuator can be improved through pulsed actuation compared to its steady counterpart. Investigations of the electric wind induced by the DBD plasma actuator in still air, when mounted on the flat plate, revealed that while the steady actuation produces an electric wind similar to a wall jet, the pulsed actuation creates a train of co-rotating vortices. The vortices are the result of a starting vortex produced by the actuator at each actuation pulse. A parametric study showed a dependence of the size, shape and propagation velocity of the vortices on the pulse frequency and duty cycle. With the actuator mounted along the apex of the cylinder, Particle Image Velocimetry measurements of the uncontrolled and controlled flow with a free-stream velocity of 5 m/s showed a clear reduction of the recirculation region downstream the cylinder when using plasma actuation. An even higher control effect could be achieved with pulsed actuation compared to the steady actuation. Phase-locked measurements of the unsteady actuation showed that pulsed actuation periodically shifted the flow separation location resulting in the propagation of vortical structures in the recirculation region. The size of the vortical structures showed a dependence on the pulsed actuation timing parameters. https://doi.org/10.1063/1.5037770

I. INTRODUCTION

Separation of boundary layers on an object moving through a fluid, such as an aircraft or a vehicle, typically means an increase in drag. In almost all cases separation is detrimental to performance. For technical applications measures are usually taken to fully avoid or at least limit the extent of separation. Such measures can be taken through a suitable geometrical design of the body, as for instance shaping an airplane wing in such a way that separation is avoided also at high angles of attack or by using some type of flow control, either passive or active. With passive control we refer to methods that do not require external power input, whereas active methods need such an input. In the latter case it could also be reactive control, *i.e.* the amount of control employed is based on information from a sensing system.

Dielectric Barrier Discharge (DBD) plasma actuators are active flow control devices with interesting features as they are easy to apply on surfaces where the flow must be controlled and the needed input power is low. The actuators are built with two electrodes asymmetrically applied on both sides of a dielectric sheet. Applying a high-frequency, high-voltage alternating current between the electrodes produces a plasma region above the dielectric sheet, *i.e.* air is ionised, and induces a wall jet

[a]Present address: Scania CV AB, Södertälje, Sweden
[b]Electronic address: ramis@mech.kth.se
[c]Electronic address: phal@mech.kth.se

often referred to as the electric wind. More precisely, when starting a plasma actuator, the flow above the actuator is accelerated and a vortex, usually referred to as the starting vortex, is formed. As the actuation continues the starting vortex moves away from the actuator and the electric wind becomes similar to a wall jet.

Whalley and Choi[1] studied the evolution of the starting vortex and showed that once the electric wind velocity reached a steady-state, the starting vortex becomes a self-similar structure. When using a DBD plasma actuator in pulsed mode, *i.e.* the actuator is turned ON and OFF at regular intervals, the starting vortex mechanism produces a train of vortices.[2] For a deeper understanding of the mechanisms responsible for the formation of the electric wind and the parametric dependence of the actuators the reader is referred to recent review paper by Benard and Moreau[3] and Kotsonis,[4] while the reviews of Moreau[5] and Wang et al.[6] summarise relevant flow control studies by means of plasma actuation, and Kriegseis et al.[7] covers the control of laminar boundary layers.

Greenblatt and Wygnanski[8] reviewed studies of flow separation control on various geometries using different control techniques and showed that the control efficiency varies depending on the relative pulse frequency to the dominant frequencies in the flow and the strength of the actuation. Pulsed actuation has shown efficiency in controlling axisymmetric wakes, *e.g.* the study of Oxlade et al.[9] showed that a high-frequency forcing significantly increases the base pressure as the curvature of the detaching streamlines change under the actuation effect and the wake became narrower. Nominally two-dimensional separation from cylinders or square-back bodies have also been controlled by pulsed actuation. The study of Jukes and Choi[10] shows a direct relation between the pulse frequency and the effect on the von Kármán vortex street downstream the cylinder; low-pulse frequencies of the order of the vortex-shedding frequency induced a lock-on effect of the vortices resulting in an increase in drag, while increasing the pulse frequency resulted in a decrease of the drag for a force input above a certain threshold value.

In the case of separating and reattaching flows two dominant frequencies can be observed; close to the separation the flow is dominated by high-frequency motions related to the Kelvin-Helmholtz instability, while inside and downstream the recirculation region a frequency of a lower order dominates due to the presence of large eddies. The low frequency is related to the 'flapping motion' of the separated shear layer. This was observed for instance experimentally by Spazzini et al.[11] and Pouryoussefi et al.[12] for backward-facing step flows, but also in simulations by Futrzynski[13] for a flow separating from a cylindrical bump. Pouryoussefi et al.[12] used pulsed DBD plasma actuation on their backward-facing step and showed that using a pulse frequency equal to that of the flapping motion resulted in the highest reduction of the reattachment length. However, Minelli et al.[14] simulated the effect of zero-net-mass flux synthetic jets and showed that increasing the pulse frequency compared to the one of the flapping motion improved the performance of the control and decreased the drag on the model. Using a frequency higher than that of the uncontrolled shear-layer frequency, on the other hand, decreases the control performance.

The present study is part of a project aiming to control turbulent flow separation occurring on geometries with strong changes in curvature that share flow features of A-pillars of truck cabins.[15] The shaping of the A-pillars has already been optimised with the introduction of rounded corners in the 80's,[16] however, flow separation still occurs at non-zero yaw angles. Due to the curved geometry the flow separation location is not fixed and active flow control methods are nowadays of interest to further improve the control of flow separation on A-pillars.[14] In order to investigate flow separation and its control with similar characteristics as A-pillars, the generic geometry of a flat plate with a cylindrical bump mounted on the plate was chosen. Such a geometry presents abrupt changes and large curvatures as well as can be used in a wind tunnel while keeping blockage effects small.

In a previous study by the authors,[17] Dielectric Barrier Discharge (DBD) plasma actuation was tested to inject momentum and control flow separation occurring on the cylindrical bump where the effect of the position of the actuator was investigated in detail for steady actuation. The study showed that the reattachment length downstream the bump could be reduced for an inlet velocity U_0 of 5 m/s. However, with the pressure measurement technique employed for that study it was not possible to investigate the detailed mechanism of flow control.

In the present study, a single DBD plasma actuator aligned in the spanwise direction is used both in steady and unsteady, also called modulated or pulsed, actuation. For the latter, the pulse frequency f_p and the duty cycle DC of the plasma actuation have been varied as the main control parameters and Particle Image Velocimetry (PIV) was employed in order to get a better understanding of the flow field and control mechanism. Prior to this, the created train of (starting) vortices has been studied in detail for different control parameters.

The paper is organised as follows: The first part describes the experimental setup including the wind tunnel, the actuators and the PIV setup. Then a study of the electric wind produced by the DBD plasma actuator when fed with either steady or pulsed power is described with special attention on the train of spanwise vortices produced by the pulsed actuation. Finally, the results of the plasma actuation on the separation bubble downstream the bump are presented.

II. EXPERIMENTAL SETUP

A. Wind-tunnel setup

The measurements were conducted in the closed-loop, low-speed BL wind tunnel[18] at the KTH Fluid Physics laboratory. The test section of the wind tunnel is 4 m long, with a cross-sectional area of 0.75×0.5 m^2 in the vertical and spanwise directions, respectively. A drawing of the test section and the setup can be seen in Fig. 1. A 3 m long and 0.02 m thick Plexiglas plate with a smooth and 0.05 m long elliptical leading edge was mounted 0.13 m beneath the roof of the test section, *i.e.* the distance between the lower side of the plate and the bottom wall of the test section is 0.6 m. This configuration was chosen in order to allow the laser sheet, used for the PIV measurements, to enter the test section through its bottom wall. For the ease of understanding, all results are, however, presented with the wall normal axis (y) directed towards the top of the page. For the study of flow separation, a $D = 2h = 0.100 \pm 0.005$ m diameter (h denoting the bump height) and 0.5 m long cylindrical bump was mounted on the lower surface of the plate with its windward edge positioned 1 m downstream the leading edge of the plate as depicted in Fig. 1. The resulting blockage ratio was 8% while the spanwise length of the bump was 10 times the height to ensure a low effect of the side-walls on the nominally two-dimensional flow. The coinciding point of the spanwise centre of the test section and the centre of the cylindrical bump was taken as the origin of the coordinate system, *i.e.* $(x, y, z) = (0, h, 0)$ corresponds to the apex of the bump at the spanwise centre of the test section.

A Prandtl tube was placed at the inlet of the test section and monitored with a pressure transducer of type *Furness FC012* to set the inlet velocity U_0 in the test section, variations lower than 1% of the velocity were observed. For this study an inlet velocity of 5 m/s is used hence the Reynolds numbers of the study based on the height of the cylinder and inlet velocity is $Re_h = 16.6 \cdot 10^3$. Two arrays of *DYMO* tape with the letter 'V' embossed, with the apex oriented in the downstream direction, were placed just downstream the elliptical leading edge of the plate and along the span in order to fix the transition location and ensure the development of a turbulent boundary layer upstream the cylindrical bump.

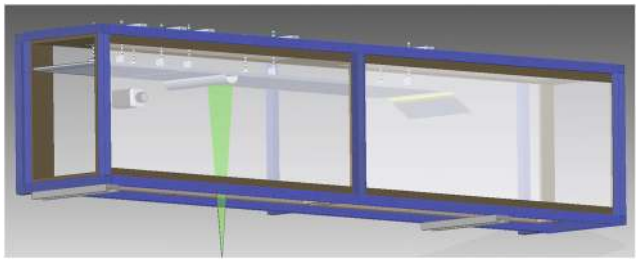

FIG. 1. Drawing of the setup with the plate and cylindrical bump mounted upside-down and attached to the top wall of the test section. The green area represents the laser sheet used for the PIV measurements and the camera can be seen placed behind the test section from the viewer point of view. This PIV configuration was used for 2D-measurements in the streamwise/wall-normal plane (xy-plane). Flow is from left to right.

B. DBD plasma actuator

The DBD plasma actuators are in-house built and made of 66 μm-thick copper electrodes applied on both sides of a 396 μm-thick dielectric sheet made of Kapton and Teflon layers. The electrodes are positioned asymmetrically, with a small overlap of 0.5 mm to ensure the formation of an homogeneous plasma along the exposed electrode.[19] A high-voltage (V_d = 12 kV$p-p$) and high-frequency (f_d = 6.5 kHz) alternating current is applied to the exposed electrode to sustain the discharge while the embedded electrode, *i.e.* the electrode encapsulated between the dielectric material and the support, is grounded. The width of the exposed electrode was 6 mm and the embedded electrode was at least 10 mm wide, to ensure that the plasma extension was not limited. For this part of the study the actuator was applied on the surface, the flat plate or the cylinder, with the electrodes aligned with the spanwise direction and an actuation length of 480 mm.

A high-frequency, high-voltage generator with a full bridge converter and a transformer cascade of type *Minipuls2* (*GBS Elektronic*) was used to feed the high-voltage, high-frequency alternating current to the DBD plasma actuator. The driving frequency f_d and the amplitude of the driving voltage V_d were controlled by external signals provided to the *Minipuls2*. A high-voltage probe (*Pintek Electronics HVP-39PRO*) connected between the high-voltage cable feeding the exposed electrode and the electrical ground and read by an oscilloscope (*Tektronix TDS*) was used to monitor f_d and V_d. To produce the pulsed actuation, the external signal input to the *Minipuls2* to control the amplitude of the driving voltage was multiplied by a square wave of the desired pulse frequency f_p and duty cycle DC. In this study, the duty cycle is defined as the percentage of time the driving voltage is non-zero; in that sense steady actuation can be seen as an actuation with a duty cycle of 100%. A picture of the screen of the oscilloscope when testing the setup with f_p = 20 Hz and DC = 50% is shown in Fig. 2.

Hot-wire anemometry measurements conducted on a similar geometry[20] downstream the reattachment location showed a dominance of structures with a Strouhal number between 0.18 and 0.26, based on the height of the cylindrical bump h and the inlet velocity U_0. This Strouhal number relates to the aforementioned 'flapping motion' frequency,[12] and was hence used to determine the pulsed frequencies which should be tested in this study: pulsed frequencies of 25, 50 and 75 Hz were chosen with duty cycles of 10, 25 and 50%. Table I summarises the Strouhal number related to the pulse frequencies. The phase angle $0 \leq \Phi_p \leq 2\pi$ is used to describe the timing of events related to the periods of the pulsed actuation, *i.e.* the actuation is always triggered at $\Phi_p = 0$. Phase-locked measurements are realised at the angles Φ equal to 0 (= 2π), $\pi/2$, π and $3\pi/2$.

To study the electric wind and the starting vortex produced by the DBD plasma actuator in still air, the actuator was fixed on the surface of the flat plate with the electrodes aligned in the spanwise direction. The total thickness of the actuator, including the dielectric layers, support and tape is

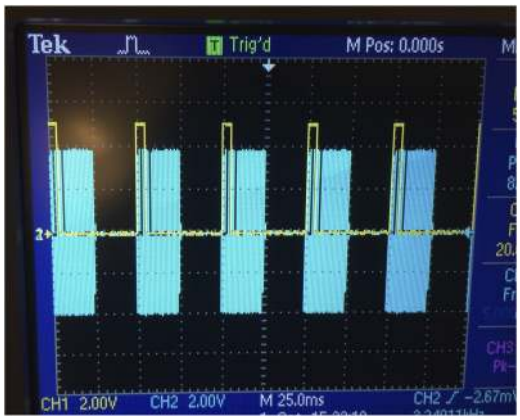

FIG. 2. Picture of the oscilloscope screen. The blue signal comes from the high-voltage probe. The pulsed frequency (f_p = 20 Hz) can be seen as the horizontal scale represents 25 ms, in this case DC = 50%. The yellow signal is synchronised on the blue signal and used to trigger the PIV system.

TABLE I. Strouhal numbers (St_h), based on the bump height h and the inlet velocity U_0, of the pulsed actuation.

U_0	Re_h	f_p = 25 Hz	f_p = 50 Hz	f_p = 75 Hz
5 m/s	$16.6 \cdot 10^3$	0.25	0.50	0.75

0.83 mm and is represented by a grey area on the figures presenting the results. The top electrode is represented by a black area, the thickness of the electrode is exaggerated for visibility purposes (see *e.g.* Fig. 3).

For the flow control study, the DBD plasma actuator was flush mounted on the surface of the cylindrical bump, *i.e.* the same layers of support, tape and dielectric material are applied all around the cylinder thus the only part of the actuator protruding from the surface was the exposed electrode. The electrodes were aligned with the spanwise direction and the downstream edge of the exposed electrode was positioned 90° from the windward edge of the cylindrical bump, *i.e.* with the apex of the bump.

C. Particle image velocimetry measurements

For this study two PIV measurement campaigns were conducted. Firstly, a study of the electric wind and the starting vortex induced by the DBD plasma actuator in still air (section III), and secondly a study of the effect of plasma actuation on the flow separation on the cylindrical bump (section IV).

For both studies a *Dantec Dynamics* system was used to carry out the PIV experiments. The system consists of a *Litron Dualpower 50-200* Nd:YAG laser and a *SpeedSense M120* CMOS camera of 12-bit with a sensor resolution of 1920×1200 pixels and a storage capacity of 1825 image pairs. The laser was placed below the test section, thus the laser sheet passed through the bottom wall of the test section, made of Plexiglas, and illuminated a plane of about 0.2×0.2 m^2 (approximately 1 mm thick) in the streamwise/wall normal direction (*xy*-plane). The camera was mounted with its axis perpendicular to the *xy*-plane as can be observed in Fig. 1 and focused on the particles illuminated by the laser sheet in order to perform two-dimensional PIV measurements of the flow.

A *Dantec Dynamics* seeding generator (*10F03 High Volume Liquid Seeder*) was used to produce particles of Diethylhexylsebacate (DEHS) with a nominal diameter of 1 μm. The particles were injected downstream the test section, at the inlet of the diffusor of the wind tunnel to ensure a good mixing. The injection occurred prior to the measurement time and stopped once the desired concentration of particles was obtained. For the study of the electric wind and starting vortex, the measurements were realised in still air. The wind-tunnel was operated at a few meters per second while injecting the particles to spread them and turned off once the particle concentration was sufficient, *i.e.* before starting the PIV measurement.

For the separation-control study, the area of interest is larger than the PIV Field-Of-View (FOV), hence the laser and the camera were mounted on a bi-directional, streamwise and spanwise directions, traversing system (*ISEL C142-4*) in order to be able to measure four successive and overlapping FOV in the streamwise direction. As the measurements of the different FOV were not simultaneous, only statistics of the total investigated area could be reconstructed; the planes were staggered next to each others with the three boundaries chosen at the positions x = 0, 0.1 and 0.25 m. Measurements were

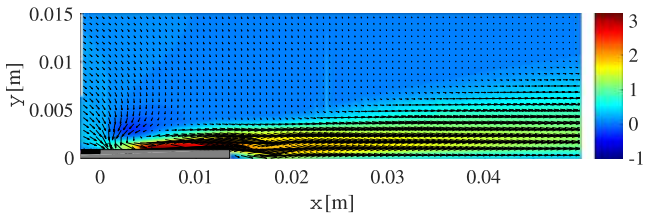

FIG. 3. Time-averaged flow produced by the DBD plasma actuator in steady mode. The colour-scale unit is meters per second and represents the streamwise component of the velocity, while the arrows represent the in-plane motion.

TABLE II. Parameters and characteristics of the PIV measurements, where 'act.' stands for actuation, 'PL' for phase-locked.

	Study of electric wind and starting vortex		Study of separation control		
FOV	0.052 m × 0.018 m		0.175 m × 0.107 m		
$\Delta x = \Delta y$	0.219 mm		0.741 mm		
Δt	74 μs		148 μs		
		Pulsed act.		Pulsed act.	
	Steady act.	PL	Baseline and steady act.	PL	Non-PL
f_s	50 Hz	f_p	200 Hz	197 Hz	f_p
N	1825	> 900	1825	1825	> 900

carried out at the spanwise position $z = 0$ m (spanwise centre) and an additional measurement was taken at $z = -0.043$ m in order to investigate the two-dimensionality of the baseline flow.

The software *DynamicStudio v4.10* was used for the acquisition and the post-processing of the PIV images. The 'one-quarter' rule was used to set the exposure time delay Δt between the images of the image-pair, *i.e.* that the particle displacement during Δt should correspond to one quarter of the interrogation window size. Both for the starting-vortex study and the separation control study, the phase-locked PIV measurements were triggered using a signal synchronised with an input signal to the power supply of the DBD plasma actuator as described before. Hence the acquisition frequency f_s of the phase-locked measurements was equal to the pulsed frequency f_p and at least 900 image-pairs were recorded. The sampling frequency and the number of samples recorded for different PIV measurements as well as the size of the FOV and the final vector spacing (Δx and Δy) are summarised in Table II. Note that a f_s of 197 Hz was selected for the separation control study when testing pulsed actuation (non phase-locked measurements) instead of 200 Hz for the other cases in order to avoid sampling with a multiple of the pulsed frequency.

A multi-pass iteration procedure was used to evaluate the instantaneous velocity fields starting with an interrogation window size of 64×64 pixels and finishing with 16×16 pixels and 50% overlap. The 'universal outlier detection' method described in Ref. 21 was used to detect eventual spurious velocity vectors; about 2% of the vectors, mainly located close to the wall, were detected as spurious. The measurement uncertainty is estimated to be of the order of 0.1 pixel[22] which represents ±0.062 m/s for the measurements with $U_0 = 5$ m/s, hence 1.3% of the inlet velocity. The vector fields were then exported and further analysed in *MATLAB* (*MathWorks*).

III. THE ELECTRIC WIND AND THE STARTING VORTEX

The electric wind produced by the actuator in the case of steady and pulsed actuation in still air was studied by varying the pulse frequency f_p and the duty cycle DC. At the initiation of the actuation and thus the start of the electric wind, a vortex, so-called starting vortex, is created with its axis aligned with the direction of the electrode. As the actuation continues, the jet develops, the starting vortex moves away from the top electrode and loses in strength and the electric wind is now similar to a wall jet as can be seen in Fig. 3.

By successively turning the DBD plasma actuator ON and OFF, *i.e.* having a pulsed actuation with a certain pulse frequency f_p and duty cycle DC, a starting vortex can be produced each time the actuator is turned ON and used for flow control. In this case a train of vortices is created as can be seen in Fig. 4. The vortices appear similar to the starting vortex produced at the beginning of a steady actuation but it is shown here that they are not identical as the vortices interact with each others.

A. Steady electric wind and momentum coefficient

The momentum coefficient c_μ used in many studies, see the review of Greenblatt et al.[8] allows a comparison and classification of active flow control methods inputting momentum into the flow and is defined as follows:

$$c_\mu = \frac{F_{act}}{1/2\rho U_0^2 L}, \tag{1}$$

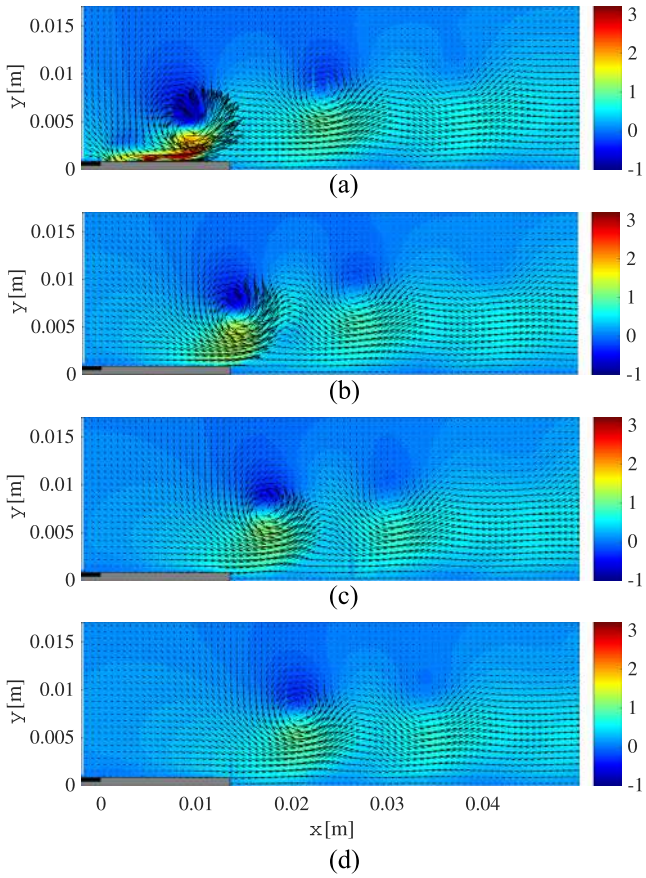

FIG. 4. Phase-locked measurements of the starting vortex in still air for f_p = 25 Hz and DC = 25%. The phase-locked measurements are carried out at $\pi/2$, π, $3\pi/2$ and 2π (a), b), c) and d) respectively). The colour-scale unit is meters per second and represents the streamwise component of the velocity, while the arrows represent the in-plane motion. a) $\Phi_p = \pi/2$. b) $\Phi_p = \pi$. c) $\Phi_p = 3\pi/2$. d) $\Phi_p = 2\pi$.

where F_{act} is the force or momentum flux of the actuation method per unit spanwise length, ρ is the fluid density and L is a characteristic length scale, taken here as the cylindrical bump height h. Greenblatt et al.[23] used this definition to evaluate the momentum coefficient c_μ of their plasma actuators running in steady mode and defined the pulsed-modulated momentum coefficient as:

$$\langle c_\mu \rangle = DC \times c_\mu \,. \tag{2}$$

These definitions are used to evaluate the momentum coefficients applied here, hence the momentum coefficient for the steady actuation needs to be evaluated first. Kriegseis et al.[24] compared different methods to evaluate the body force produced by DBD plasma actuators using velocity data. Using the control volume method, having the electric wind directed from left to right (see e.g. Fig. 3), and assuming a two-dimensional, steady and incompressible electric wind, the body force per unit span can be evaluate as:

$$F_{act} = \left\langle \int_{\text{right}} \rho u_e^2 \mathrm{d}y - \int_{\text{left}} \rho u_e^2 \mathrm{d}y + \int_{\text{top}} \rho u_e v_e \mathrm{d}x + \int_{\text{wall}} \tau_w \mathrm{d}x \right\rangle, \tag{3}$$

where u_e and v_e are the streamwise and wall-normal components of the electric wind velocity, respectively, τ_w is the wall shear stress, and the angle brackets indicate the time-average operator. The respective boundaries of the rectangular control volume are indicated by right, left, top and wall. Kriegseis et al.[24] evaluated the influence of the position of the right boundary and showed that while moving the right vertical boundary downstream, the body force increases until it reaches a plateau. As long as the body force increases, the momentum through the right boundary is almost equal to

the body force per unit length but then it starts decreasing as the wall shear stress increases. Thus in this study, the average of the momentum of each instantaneous velocity field at the right boundary is evaluated for different positions of the boundary and the maximum is taken as the body force per unit span.

A body force per unit span of 10.4×10^{-3} N/m was found for the steady actuation which results in a momentum coefficient c_μ of 1.4%. A note of caution should be added; the PIV setup was designed to observe the train of vortices produced by the pulsed actuation hence the FOV is too large to accurately resolve the thin electric wind jet produced by the steady actuation of the plasma actuator.

B. Train of vortices created by pulsed actuation

Figure 4 shows that a train of vortices is created by the pulsed actuation of the DBD plasma actuator. In this case f_p = 25 Hz and DC = 25%, so the actuation is on for $0 < \Phi_p \leq \pi/2$. It can be observed that a vortex similar to a starting vortex is created downstream of the top electrode of the DBD plasma actuator and is then moving downstream. For the FOV of the PIV experiments, the motion of the vortex can be studied over two periods as a vortex downstream the starting vortex being created is visible in Fig. 4a); this is the vortex created during the previous pulse.

Figure 5 shows the evolution of the streamwise position of the centre of the vortices, x_c, which were extracted visually from the vector fields, created by the pulsed actuation as a function of the phase angle for different f_p and DC. For some cases, 8 data points are available as two vortices are visible for all 4 phases measured within the FOV. In other cases, the strength of the vortex decreases during the second period, the lower part of the vortex (which has a velocity in the direction of the electric wind) is stronger than the higher part of the vortex, which then becomes wavy and no centre of the vortex can be detected. The figure shows that at the same frequency, vortices created with a longer duty cycle are carried downstream faster. When the frequency increases, the distance travelled by the vortex during one period decreases and the vortex remains closer to the actuator when the actuation is turned on again.

A linear relation is used to fit all the data points available in Fig. 5a) and only the first four data points in Fig. 5b). Indeed an irregularity can be observed for the centre position between the phases $\Phi_p = 2\pi$ and $5\pi/2$. This irregularity is hardly discernible for the measurements with f_p = 25 Hz, but becomes more apparent with increasing frequency. It is due to the fact that at $\Phi_p = 2\pi$ the DBD plasma

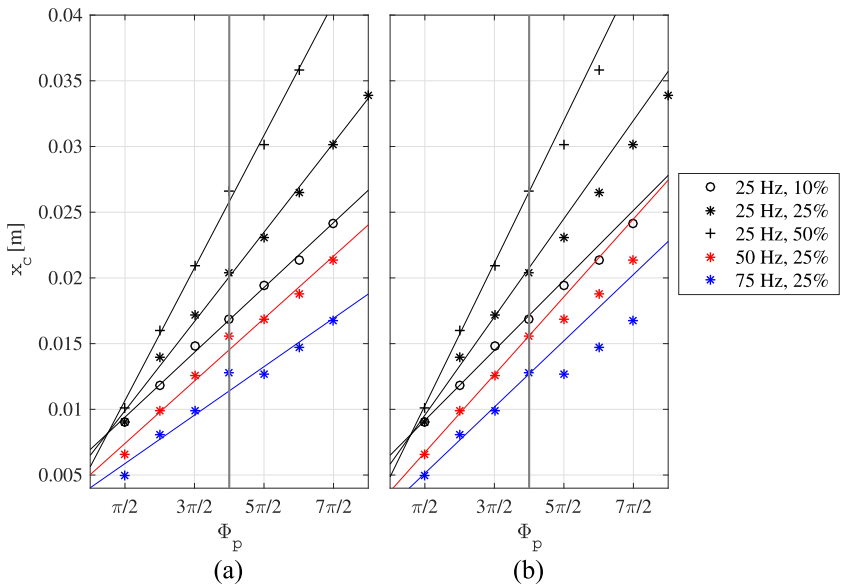

FIG. 5. Streamwise position of the vortex centre as a function of the phase angle for different pulsed frequencies and duty cycle. The lines represent linear fits to the experimental data. In a) all data points are used to determine the linear relation of each case, while in b) only the first four points, *i.e.* $\pi/2 \leq \Phi_p \leq 2\pi$, are used. The grey vertical lines are plotted at $\Phi_p = 2\pi$ and separate the first from the second period.

actuator is turned on again, a new vortex is created and has the effect to decrease the propagation speed of the vortex formed during the previous period. As the frequency increases, the vortex created during the previous period is closer to the actuator when the actuation is initiated again. This is more visible for the cases with $f_p = 50$ and 75 Hz, while for the latter it seems that the vortex is even pulled back as x_c decreases between $\Phi_p = 2\pi$ and $5\pi/2$. This explains why the linear relation is a better fit when using only the four first points of the centre measurements and is then used to evaluate the propagation velocity of the starting vortex. Fig. 6 shows the propagation velocity, *i.e.* the coefficient of the linear fit multiplied by $360 \times f_p$, using all data points U_{e1}, thus corresponding to the linear fit in Fig. 5a) and using only the first four points U_{e2} (Fig. 5b)). It can be seen that as already observed the propagation velocity increases with the duty cycle, the propagation velocity also increases with the frequency.

In Fig. 7, the vorticity of the phase-locked measurements at Φ_p of the starting vortex, produced with different f_p and DC, is presented. The magnitude of the vorticity seems to differ between the different cases due to variations of the vortex size. Indeed as f_p increases, the size of the starting vortex decreases as can be seen by comparing Fig. 7b), d) and f) but the vorticity increases. The size of the vortex is hence related to the actuation time, the time during which the actuator is turned ON, which decreases when considering cases with identical DC but increasing f_p. When turning the actuator ON, it takes a small transient time for the electric wind to increase and reach a stable speed.[1] The average of the maximum velocity measured for each instantaneous flow field of the phase-locked measurements is presented in Fig. 8 and shows that for all measurements with $DC = 25\%$, at $\Phi_p = \pi/2$, the electric wind speed reaches its stable velocity, about 3.7 m/s. However, it is safe to say that the stable stage has been reached for a shorter time when increasing the frequency affecting the size of the vortex. Moreover, increasing the frequency also affects the wall-normal location of the vortex centre, *i.e.* the region with high positive vorticity, which remains closer to the wall.

Comparing cases with the same f_p but increasing DC in Fig. 7a), b) and c), shows that the duty cycle affects both the size and the shape of the vortex. Looking closer to the case with $DC = 10\%$, the magnitude of the vorticity in the centre of the vortex is of the same order as with a higher DC, however, the size of the vortex, *i.e.* the region of non-zero velocity, appears larger. The maximum velocity of the flow shown in Fig. 8 is considerable smaller for the case with $DC = 10\%$. It can not be concluded that the electric wind did not reach the stable speed mentioned earlier. Indeed, the first measurement over the period is at $\Phi_p = \pi/2$ hence the plasma actuation is OFF at the time of the measurement and it can be observed for the other cases that, once the actuation is turned OFF, the maximum speed in the flow decreases rapidly. The reason for the vortex to be smaller is thus probably the same as when increasing the frequency, if the electric wind reached its stable speed during the actuation, it remained in the stable region for a shorter period of time and the vortex did not grow as much as with higher DC. When comparing cases with $DC = 25$ and 50% in Fig. 7b) and c) it can be noticed that even though the actuation has been on for the same period of time at the instant of the

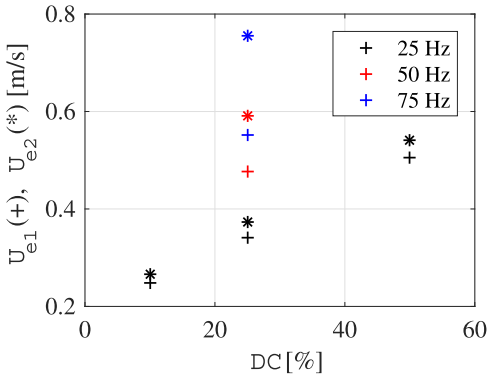

FIG. 6. Streamwise component of the propagation velocity for the starting vortex using all data points U_{e1} (+) and using only data from the first period, U_{e2} (*).

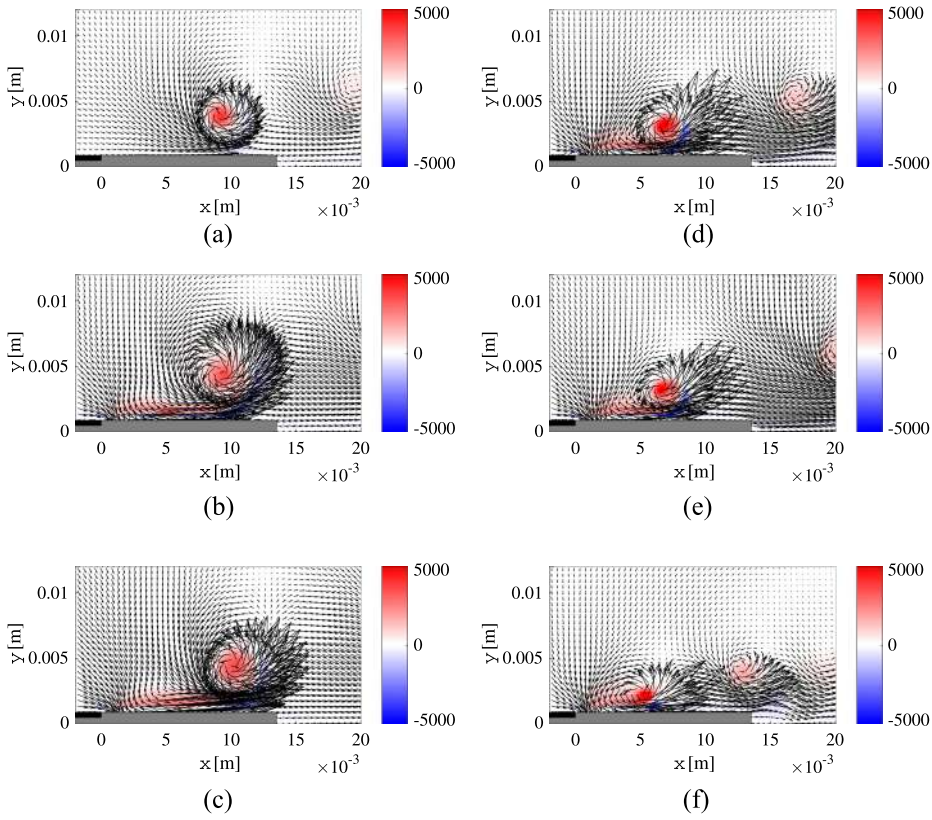

FIG. 7. Phase-locked measurements of the starting vortex in still air at $\Phi_p = \pi/2$ for different f_p and DC. The colour-scale represents the unscaled vorticity in $[1/s]$, while the arrows represent the in-plane motion. a) f_p = 25 Hz, DC = 10%. b) f_p = 25 Hz, DC = 25%. c) f_p = 25 Hz, DC = 50%. d) f_p = 50 Hz, DC = 25%. e) f_p = 50 Hz, DC = 50%. f) f_p = 75 Hz, DC = 25%.

measurement, the size of the vortices is similar but the shape differs; in the case of the highest DC, the velocity vectors are less axisymmetric than in the case of $DC = 25\%$.

Figure 9 shows the velocity profile, streamwise and wall-normal components, of the flow at the streamwise position $x = 0.1$ m and $\Phi_p = 2\pi$, *i.e.* just prior to the start of a new pulse. For all cases presented, the velocity did not decrease to zero and for higher DC the streamwise velocity is larger and affects a larger region above the wall. This remaining flow from the vortex, which moved downstream, affects the formation of the new vortex and explains the polarisation of the velocity vectors in Fig. 7c). The influence of the previous vortex on the formation of the new vortex seems to become stronger as the frequency increases as can be seen in

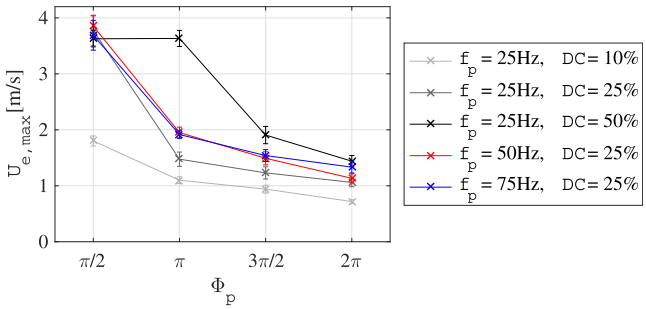

FIG. 8. Comparison of the maximum streamwise velocity close to the wall for different pulsed conditions. The error bar represents the standard deviation.

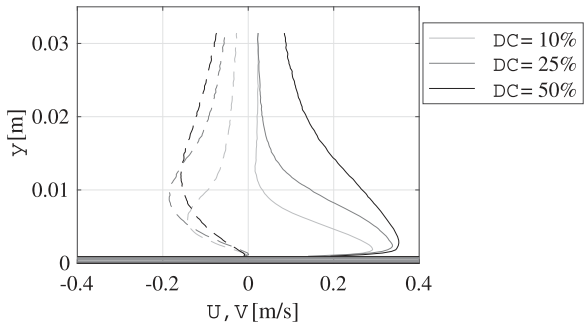

FIG. 9. Comparison of the streamwise (line) and wall-normal (dashed-line) components of the velocity at x = 0.01 m and $\Phi_p = 2\pi$ (just before a new pulse starts) for the cases with f_p = 25 Hz and duty cycle DC = 10, 25 and 50%.

Fig. 7d), e) and f). The present observations are therefore well in line with previous characterisation studies.[2,25]

IV. RESULTS ON SEPARATION CONTROL

In this section the results from the study of the turbulent boundary layer approaching and separating on the cylindrical bump as well as the control of the recirculation region using the DBD plasma actuator are described. The base flow is shown in Sec. IV A. The following subsections show the effect of the pulsed actuation compared to the baseline flow and the steady actuation, starting by comparing the effect of varying the pulse frequency in Sec. IV B and the duty cycle in Sec. IV C.

A. Baseline flow

The baseline flow is shown in Fig. 10. The mean flow is reconstructed from the measurements of four different FOV as described above. Furthermore, Fig. 10b) shows the profile of the mean streamwise component of the velocity as well as the Reynolds stresses at the location $x = -0.1$ m, *i.e.* upstream the cylinder. At this position the turbulent boundary layer is affected by an adverse pressure gradient and a flow separation with a small recirculation region is visible in Fig. 10a) at the windward edge of the bump. The flow then reattaches and is accelerated as it passes the forward facing side of the bump. However, when the curvature of the streamlines changes from concave to convex, the flow experiences a change in curvature and a strong adverse pressure gradient which makes the flow to separate from the bump. Indeed, as Simpson[26] summarises in his review, a flow under the effect of a similar adverse pressure gradient, but developing on a flat plate would detach from the surface further downstream. Simpson[26] explains that it is due to the sudden increase of the cross-sectional area and the fact that the flow away from the surface cannot follow the change in curvature, hence the flow velocity near the wall decreases rapidly to fulfil mass conservation. Finally a third recirculation

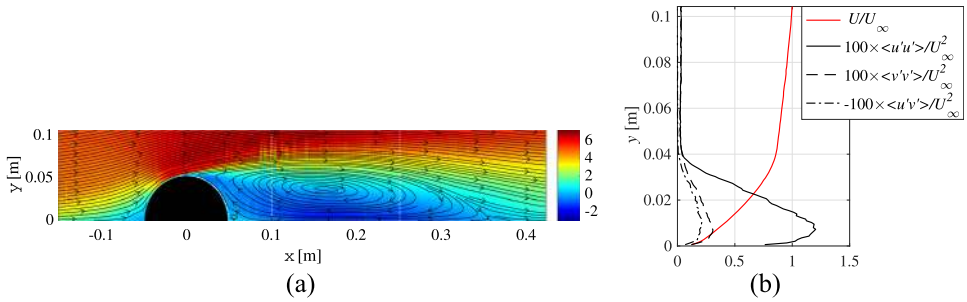

FIG. 10. a) Mean flow of the baseline case at U_0 = 5 m/s. The colour-scale is in meters per second and shows the streamwise component of the velocity, the streamlines show the in-plane flow motion. b) Time-averaged streamwise velocity and Reynolds stresses of the turbulent boundary layer approaching the cylindrical bump (x = -0.1m) at U_0 = 5 m/s.

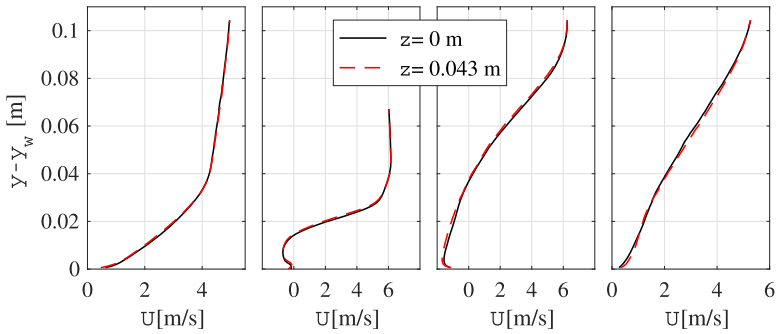

FIG. 11. Comparison of mean streamwise velocity profiles of the baseline flow at $z = 0$ m and $z = 0.043$ m and at the streamwise locations, from left to right, x = -0.1 m, 0.035 m, 0.17 m and 0.4 m. $U_0 = 5$ m/s.

region can be observed at the corner between the plate and the trailing edge of the cylindrical bump due to the backflow from the large recirculation region.

In Fig. 11, the mean streamwise velocity at different streamwise locations is compared for the measurements along the spanwise centre of the test section (z = 0 m) and the spanwise location $z = 0.043$ m. The profiles collapse on top of each other at each streamwise location studied ensuring the two-dimensionality of the flow around the centreline of the test section and that no effect from

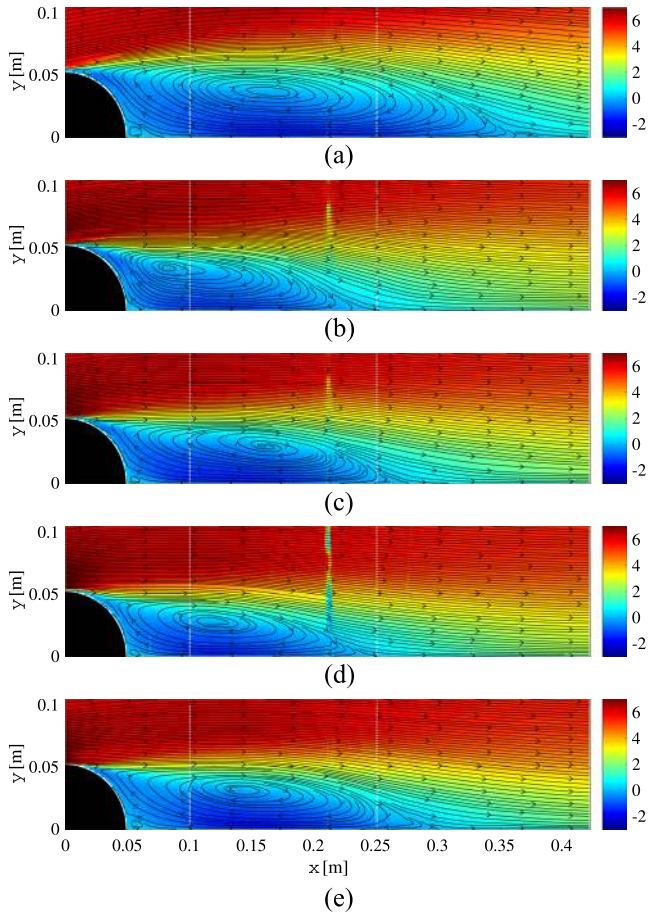

FIG. 12. Mean flow of the baseline case (a), pulsed actuation with different frequencies and $DC = 25\%$ (b)–d)) and the steady actuation. The colour-scale unit is m/s and represent the streamwise component of the velocity, while the streamlines indicate the in-plane motion. a) Baseline. b) f_p = 25 Hz. c) f_p = 50 Hz. d) f_p = 75 Hz. e) Steady.

boundary layers on the side-walls can be observed here. Note that in a related study[27] the spanwise homogeneity was shown to be at least twice as large as shown here.

B. Effect of the pulse frequency on the control

The control effect on the recirculation area can be seen in Fig. 12 were the mean streamwise component of the velocity is presented along with streamlines to indicate the in-plane flow motion of the baseline flow as well as the controlled flow with f_p = 25, 50 and 75 Hz at a *DC* of 25% and the controlled flow with steady actuation. Some of the figures show spurious data around x = 0.2 m caused by a distortion of the PIV-laser sheet when passing through a joint in the test section. The DBD plasma actuator is seen to increase the streamwise velocity on top of the cylinder (see Fig. 12b)–e)) and influences the separation location on the cylinder to move downstream. The reattachment location on the plate, on the other hand, has moved upstream for all types of actuation. Moreover, the pulsed actuation seems to be more effective than the steady actuation in shortening the recirculation area. Although the recirculation area seems to be of comparable length for the different controlled cases with pulsed actuation, the centre of the recirculation bubble as well as the curvature of the streamlines in the shear layer differ from one case to another.

To be able to study in more detail the effect and the differences between the different actuation methods, Fig. 13 shows the mean streamwise velocity as well as the Reynolds stresses of the flow cases shown in Fig. 12 at three different streamwise locations; on the cylinder, in the

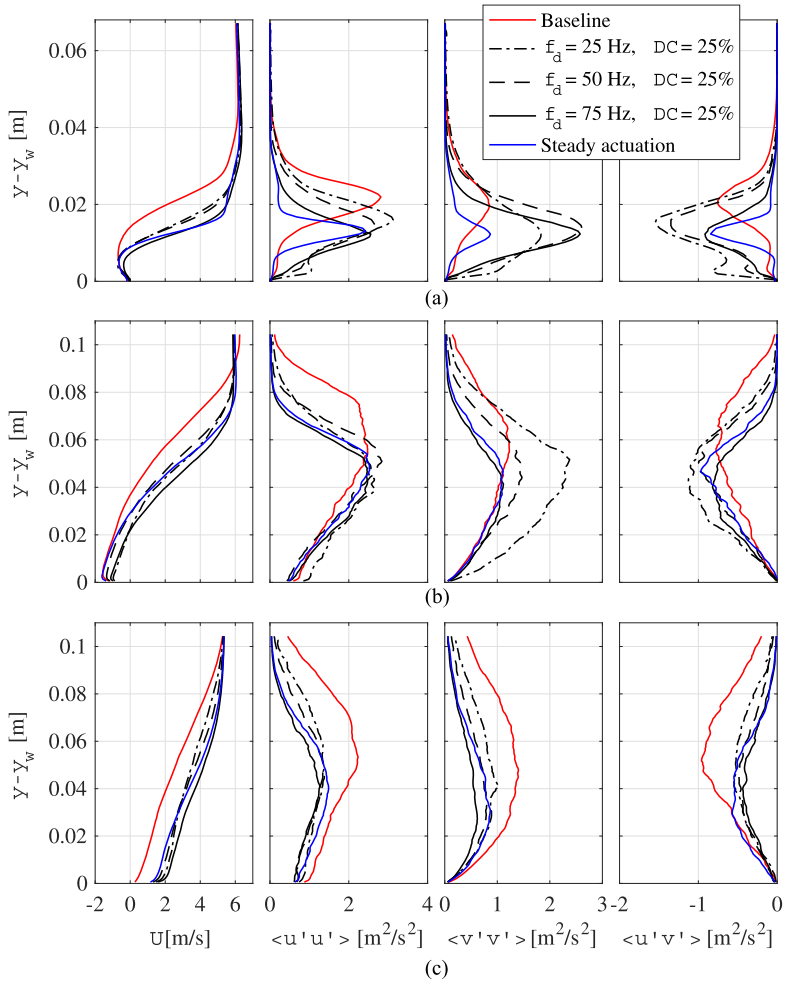

FIG. 13. From left to right comparison of the time-averaged streamwise component of the velocity and the normal and shear stresses of the baseline flow and different actuation cases at x = 0.035, 0.17 and 0.4 m, a), b) and c), respectively.

recirculation area and downstream the reattachment (x = 0.035, 0.17 and 0.4 m in Fig. 13a), b) and c), respectively).

The velocity profile at x = 0.035 m (Fig. 13a)) can be used to study the capacity of the actuation to delay the separation location. Indeed, as the profile is measured close to the separation, a lower wall-normal location of the zero-crossing indicates that the flow separated further downstream. The profiles confirm the previous conclusions; the actuation delays the separation of the flow especially the cases with steady actuation and actuation at the highest frequency (f_p = 75 Hz). Furthermore, comparison of the Reynolds stresses at this streamwise location shows a strong increase of the turbulence level when using pulsed actuation, whereas the amplitude of the Reynolds stresses is of the same order in the baseline and the steady actuation cases. The amplitude of $\langle u'v' \rangle$ decreases with f_p, in the case of the highest frequency.

The profiles in the recirculation bubble (Fig. 13b)) at x = 0.17 m show that the high amplitude of the Reynolds stresses expand further away from the wall for the baseline flow than when using plasma actuation since the recirculation region is thicker. This is also confirmed by the mean profiles of the streamwise velocity. The maximum amplitude of the Reynolds stresses are comparable for all flow cases except for $\langle v'v' \rangle$ of the actuation with f_p = 25 Hz, which exhibits larger values. Furthermore, the mean streamwise velocity profiles at x = 0.4 m (Fig. 13c)) confirm that the reattachment of the flow occurs further upstream when using DBD plasma actuation and explains the lower magnitude of the Reynolds stresses for the actuated flow compared to the baseline flow.

Figure 14 shows streamlines of phase-locked measurements of the pulse-actuated cases with f_p = 25 and 50 Hz and DC = 25% at the phase angles $\Phi_p = \pi/2$, π, $3\pi/4$ and 2π, where the plasma actuator is turned ON for $0 < \Phi_p \leq \pi/2$. Clear spanwise vortices are observed here from the streamlines. Note that the vortices are rotating in the clockwise direction, which is the opposite direction as compared to the starting vortex, hence the vortex motion seen is not in itself a result of the starting vortex.

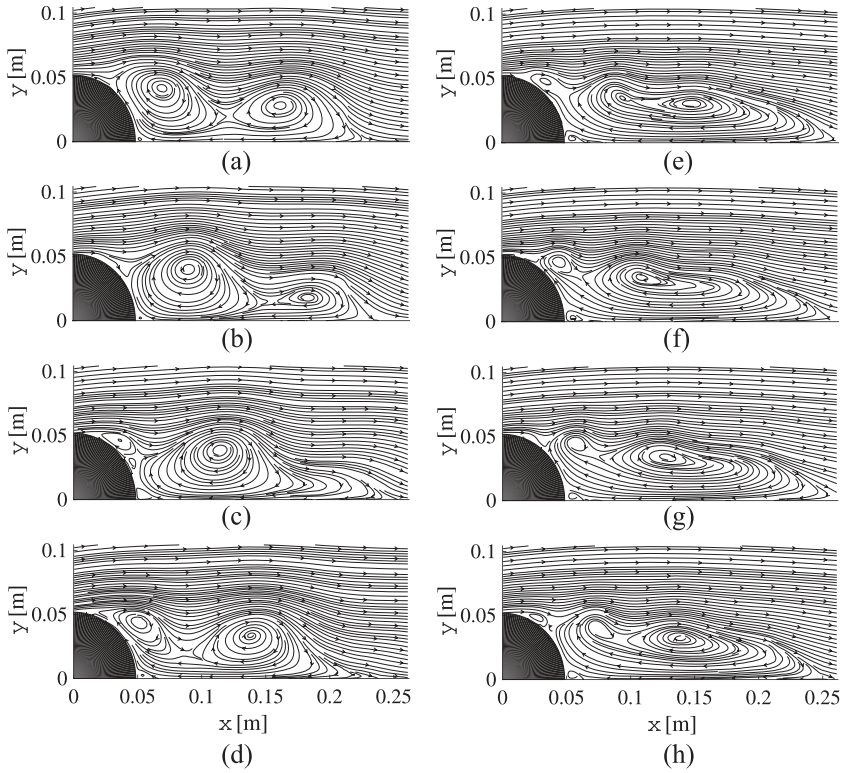

FIG. 14. Streamlines from phase-locked measurements of the case actuated at f_p = 25 Hz (a)-d)) and f_p = 50 Hz (e)-h)) with DC = 25%. Flow from left to right. a) $\Phi_p = \pi/2$. b) $\Phi_p = \pi$. c) $\Phi_p = 3\pi/2$. d) $\Phi_p = 2\pi$. e) $\Phi_p = \pi/2$. f) $\Phi_p = \pi$. g) $\Phi_p = 3\pi/2$. h) $\Phi_p = 2\pi$.

For both frequencies, the separation of the streamlines from the cylindrical bump is delayed further downstream when the actuator is turned ON (Fig. 14a) and e)) pushing the recirculation bubble downstream. A change of the orientation of the streamlines curvature above the cylinder can be noticed in both cases (Fig. 14a) and e)) and occurs at a slightly more downstream location for f_p = 25 Hz than for f_p = 50 Hz. A similar phenomenon was observed by Jukes and Choi[10] and Greenblatt and Wygnanski.[23] When the actuation is turned OFF, the separation location moves back upstream as a small recirculation bubble develops on the surface of the cylinder at first independent from the large recirculation region (*e.g.* visible in Fig. 14c) at x = 0.04 m and y = 0.04 m) and grows until the end of the period and the actuator is turned ON again.

The effect on the recirculation region is altered when changing the pulse frequency; in the case of f_p = 25 Hz, which is close to the frequency of the 'flapping motion', the actuation affects the whole recirculation region energising large vortical structures. However, when increasing the frequency the actuation effect is more localised to the upper shear layer where the pulse actuation results in the successive formation of smaller vortices convected across the free shear layer. With a lower pulse frequency, at the same *DC*, both the time period during which the actuation is ON and OFF is longer resulting in two effects on the wake: the separation line is moved further downstream during the actuation time, which could be linked to the previous observation that the starting vortex propagated further downstream during the actuation time with lower f_p as shown in Fig. 7. The second effect is due to the longer time period during which the actuator is OFF; the new recirculation bubble created on the cylinder surface can grow larger as can be clearly seen in Fig. 14d) and h).

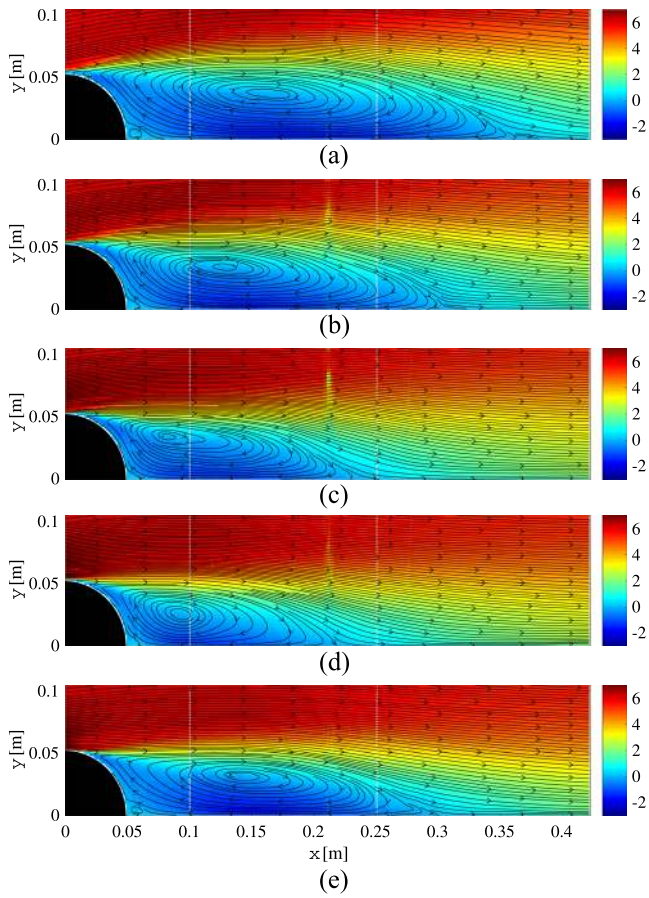

FIG. 15. Mean flow of the baseline case (a), pulsed actuation with different duty cycles and f_p = 25 Hz (b)–d)) and the steady actuation. The colour-scale unit is m/s and represent the streamwise component of the velocity while the streamlines indicate the in-plane motion. a) Baseline. b) *DC* = 10%. c) *DC* = 25%. d) *DC* = 50%. e) Steady.

C. Effect of the duty cycle on the control

In the following the effect of the duty cycle on the control efficiency of the spanwise plasma actuator will be demonstrated. In the previous section all results were for a *DC* equal to 25%, here, instead, we compare the results for *DC* equal to 10%, 25% and 50% all with f_p = 25 Hz. They are also compared with the baseline case (*i.e.* no actuation) and the steady actuation (*i.e.* *DC*=100%). This means that several graphs from the previous section are repeated here, but this merely is done for ease of comparison.

In Fig. 15 the mean streamwise velocity is depicted in colour together with streamlines showing the in-plane motion for the three values of the duty cycle as well as the baseline case and the steady actuation. As can be seen all actuated cases show a shorter recirculation region when compared to the baseline case. For *DC* = 50% the length of the separated region is the smallest and has decreased with almost 50% as compared to the baseline case. In all cases the maximum height of the separated region is also smaller than for the baseline case.

More details on the flow field can be found in Fig. 16, where velocity and Reynolds-stress profiles are shown for the five cases for three different x-positions, x = 0.035, 0.17 and 0.4 m. Already at the first position the effect of actuation can be seen, namely the vertical extent of the backflow region is smaller and the maximum of the Reynolds stresses are found closer to the cylinder wall, showing that the shear layer is less detached from the cylinder. However, all profiles show negative streamwise velocities close to the cylinder surface. The wall-normal variance and Reynolds shear stress ($\langle v'v' \rangle$

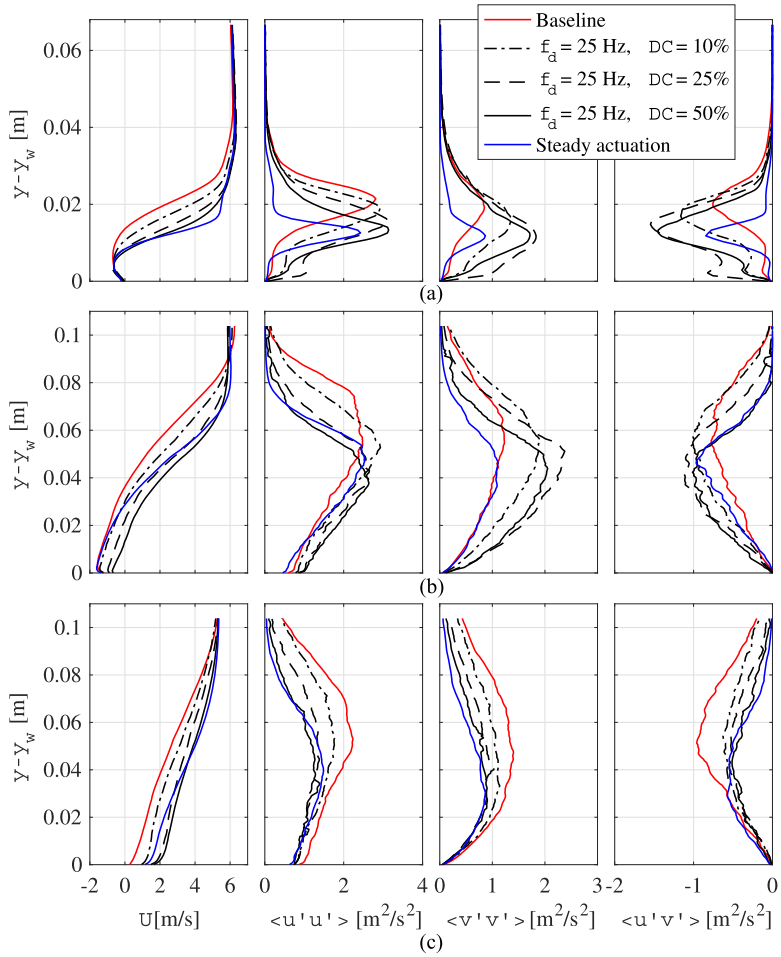

FIG. 16. From left to right comparison of the time-averaged streamwise component of the velocity and the normal and shear stresses of the baseline flow and different actuation cases at x = 0.035, 0.17 and 0.4 m, a), b) and c), respectively.

and $\langle -u'v' \rangle$, respectively) show, on the other hand, higher values with actuation indicating a stronger mixing. Increasing the *DC* further delays the separation location as the backflow region close to the wall becomes thinner. As expected the shear layer is seen to have spread in the normal direction at $x = 0.17$ m, but otherwise the picture of the Reynolds stresses from $x = 0.035$ m is repeated. However, at $x = 0.40$ m all shown Reynolds stresses are now smaller than for the baseline case, indicating that reattachment has occurred for smaller x-values in the actuated cases and that the relaxation towards a standard turbulent boundary layer has been ongoing for a longer stretch.

Phase-locked measurements at four instances during the actuation cycle are shown in Fig. 17 for two *DC* values, *i.e.* 10% and 25%. For the 10% case the actuation stops at $\Phi_p = \pi/5$, whereas for the 25% case it stops at $\Phi_p = \pi/2$. As can be seen from Fig. 17 there are similarities, but also differences, between the two cases.

Considering the large scales, it can be seen that the vortices move faster downstream for the 25% case as compared to the 10% case in accordance with Fig. 5. This also means that the vortex cores are less separated for the higher *DC* cases, probably because there is a stronger interaction between the vortices in that case. The same mechanism as described when comparing pulse frequencies can be observed here as the separation is moved further downstream when the actuation is ON and an independent recirculation bubble develops on the surface of the cylinder once the actuation is turned OFF. For the low *DC* case one can already see a tendency of separation at the cylinder surface at $\Phi_p = \pi/2$ and it becomes clearly visible at $\Phi_p = \pi$. For the higher *DC*s a similar small separated region on the cylinder is observed at $\Phi_p = 3\pi/2$. When comparing different pulse frequencies, the size of the vortical structures was shown to be dependent on the actuation timing. This is confirmed here as large spanwise vortices can be observed due to the long OFF time of the actuator between each pulse, however even though the OFF time is longer for the case with $DC = 10\%$ than with $DC = 25\%$, the vortical structures are smaller for the first case and do not evolve independently as when $DC = 25\%$, but is part of a larger recirculation region.

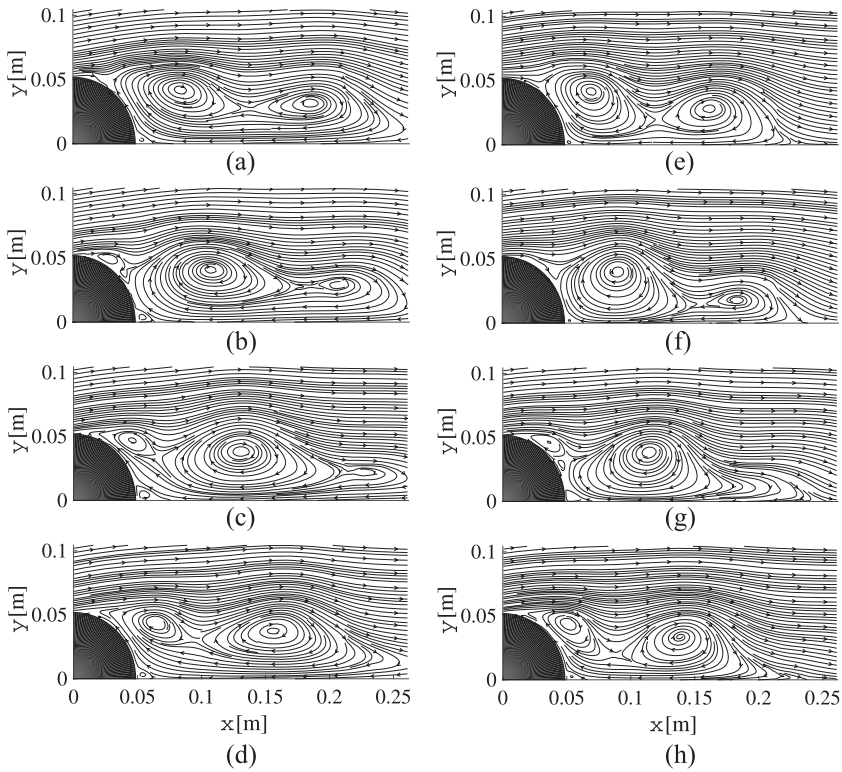

FIG. 17. Streamlines from phase-locked measurements of the case actuated at $f_p = 25$ Hz with $DC = 10\%$ (a)-d)) and $DC = 25\%$ (e)-h)). Flow from left to right. a) $\Phi_p = \pi/2$. b) $\Phi_p = \pi$. c) $\Phi_p = 3\pi/2$. d) $\Phi_p = 2\pi$. e) $\Phi_p = \pi/2$. f) $\Phi_p = \pi$. g) $\Phi_p = 3\pi/2$. h) $\Phi_p = 2\pi$.

V. SUMMARY AND CONCLUSION

The separation control effect of a DBD plasma actuator mounted at the top of a cylindrical bump has been investigated. The main focus of the study has been to evaluate if the effect of the actuator can be improved through pulsed actuation. Actuation parameters that have been varied for the pulsed case are the frequency of actuation and the duty cycle, *i.e.* the time between the actuation pulses and the pulse duration, respectively.

The study of the electric wind induced by the DBD plasma actuator in still air shows that when used in pulse mode, the actuator produces a train of co-rotating vortices. The results confirmed that the production of starting vortices in pulse mode can influence the shape and the downstream propagation of the vortices as the flow on the actuator does not relax back to zero velocity before a new vortex is created. This result is of course very dependent on the pulse frequency. The size of the vortices is also directly dependent on the pulse frequency as well as the duty cycle which could be a limiting factor for the use of pulsed DBD plasma actuators if a high pulse frequency is needed.

Clear differences were observed for the measurements between all actuated cases compared to the baseline case in terms of the length and height of the separated region. When varying the pulse frequency the highest tested pulse frequency resulted in the strongest control effect *i.e.* reduction of the size of the recirculation region. Increasing the duty cycle also reduced the size of the recirculation bubble. The phase-locked measurements showed a similar behaviour for the different pulse frequencies and duty cycles tested, *i.e.* the pulse actuation creates an oscillation of the separation location resulting in the production of vortical structures convected downstream. The size of the vortical structures is however dependent on the pulse actuation parameters. A particular situation seems to happen for f_p = 25 Hz and DC = 25%, where the vortical structures seems to evolve 'independently', *i.e.* they are not part of a larger recirculation region as for the other cases studied with phased-locked measurements. This phenomenon is probably amplified when increasing the DC to 50%.

Measurements at U_0 =10 m/s with the same force of the actuation per unit spanwise width were also performed but indicated a diminishing effect of the control efficiency. It is unclear whether this reduction in control efficiency might partially be overcome by keeping the momentum coefficient constant, however, this is beyond the scope of the present study. To overcome the known drawback of DBD plasma actuators when utilising them to inject momentum, namely their low-velocity limitation,[28] the actuators can be used as vortex generators (DBD-VG) by orienting them parallel to the flow direction.[29,30] The thereby generated strong streamwise vortices are more effective in shortening the reattachment length both on a cylindrical bump,[27] but also in a proof-of-concept study on the A-pillar of a scale model of a tractor-trailer combination.[15]

The conclusion of the present study is that plasma actuators producing an electric wind directly along the flow streamwise direction can be used for separation flow control and that pulsed actuation can be more effective than steady actuation. However, their effectiveness is limited to low-speed flow-control studies when used in such a configuration as the momentum input of such actuators remains very low.

ACKNOWLEDGMENTS

The work was financially supported by the Swedish Energy Agency within the project Flow Research on Active and Novel Control Efficiency (FRANCE), project number 34186-1. Per Elofsson and Guillaume Mercier of Scania CV AB and Gunilla Efraimsson and Romain Futrzynski from KTH Aeronautical and Vehicle Engineering (Linné FLOW Centre) are acknowledged for useful input to the project. HAL acknowledges support from the Swedish Foundation for Strategic Research (SSF) under its Strategic Mobility Program for project DRACO (Drag Reduction And COntrol). Tomas Modéer from KTH Electrical Energy Conversion, is greatly acknowledged for his help with the electrical setup.

[1] R. D. Whalley and K. S. Choi, "The starting vortex in quiescent air induced by dielectric-barrier-discharge plasma,," J. Fluid Mech. **703**, 192 (2012).

[2] M. Kotsonis and S. Ghaemi, "Experimental and numerical characterization of plasma actuators in continuous and pulsed actuation," Sens. Actuators, A **187**, 84 (2012).

[3] N. Benard and E. Moreau, "Electrical and mechanical characteristics of surface AC dielectric barrier discharge plasma actuators applied to airflow control," Exp. Fluids **55**, 1846 (2014).
[4] M. Kotsonis, "Diagnostics for characterisation of plasma actuators," Meas. Sci. Technol. **26**, 092001 (2015).
[5] E. Moreau, "Airflow control by non-thermal plasma actuators," J. Phys. D: Appl. Phys. **40**, 605 (2007).
[6] J.-J. Wang, K. S. Choi, L.-H. Feng, T. N. Jukes, and R. D. Whalley, "Recent developments in DBD plasma flow control," Prog. Aerosp. Sci. **62**, 52 (2013).
[7] J. Kriegseis, B. Simon, and S. Grundmann, "Towards in-flight applications? A review on dielectric barrier discharge-based boundary-layer control," Appl. Mech. Rev. **68**, 020802 (2016).
[8] D. Greenblatt and I. J. Wygnanski, "The control of flow separation by periodic excitation," Prog. Aerosp. Sci. **36**, 487 (2000).
[9] A. R. Oxlade, J. F. Morrison, A. Qubain, and G. Rigas, "High-frequency forcing of a turbulent axisymmetric wake," J. Fluid Mech. **770**, 305 (2015).
[10] T. N. Jukes and K. S. Choi, "Flow control around a circular cylinder using pulsed dielectric barrier discharge surface plasma," Phys. Fluids **21**, 084103 (2009).
[11] P. G. Spazzini, G. Iuso, M. Onorato, N. Zurlo, and G. M. Di Cicca, "Unsteady behavior of back-facing step flow," Exp. Fluids **30**, 551 (2001).
[12] S. G. Pouryoussefi, M. Mirzaei, and M. Hajipour, "Experimental study of separation bubble control behind a backward-facing step using plasma actuators," Acta Mech. **226**, 1153 (2014).
[13] R. Futrzynski, Ph.D. thesis, KTH Royal Institute of Technology (2017).
[14] G. Minelli, S. Krajnovic, B. Basara, and B. R. Noack, "Numerical investigation of active flow control around a generic truck A-pillar," Flow Turbul. Combust. **97**, 1235 (2016).
[15] J. A. Vernet, R. Örlü, D. Söderblom, P. Elofsson, and P. H. Alfredsson, "Plasma streamwise vortex generators for flow separation control on trucks," Flow Turbul. Combust. **100**, 1101 (2018).
[16] K. R. Cooper, "The effect of front-edge rounding and rear-edge shaping on the aerodynamic drag of bluff vehicles in ground proximity," SAE Tech. Paper (1985).
[17] J. A. Vernet, R. Örlü, and P. H. Alfredsson, "Separation control by means of plasma actuation on a half cylinder approached by a turbulent boundary layer," J. Wind. Eng. Ind. Aerod. **145**, 318 (2015).
[18] B. Lindgren and A. V. Johansson, Tech. Rep., Royal Institute of Technology, Department of Mechanics (2002).
[19] M. L. Post and T. C. Corke, "Separation control on high angle of attack airfoil using plasma actuators," AIAA J. **42**, 2177 (2004).
[20] J. A. Vernet, R. Örlü, and P. H. Alfredsson, in *Progress in Turbulence VI*, edited by J. Peinke, G. Kampers, M. Oberlack, M. Waclawczyk, and A. Talamelli (Springer International Publishing, 2016), pp. 279–283.
[21] J. Westerweel and F. Scarano, "Universal outlier detection for PIV data," Exp. Fluids **39**, 1096 (2005).
[22] M. Raffel, C. E. Willert, S. Wereley, and J. Kompenhans, *Particle Image Velocimetry: A practical guide* (Springer, Berlin, Heidelberg, 2007).
[23] D. Greenblatt, T. Schneider, and C. Y. Schüle, "Mechanism of flow separation control using plasma actuation," Phys. Fluids **24**, 077102 (2012).
[24] J. Kriegseis, C. Schwarz, C. Tropea, and S. Grundmann, "Velocity-information-based force-term estimation of dielectric-barrier discharge plasma actuators," J. Phys. D: Appl. Phys. **46**, 055202 (2013).
[25] I. Maden, J. Kriegseis, S. Jakirlic, C. Schwarz, S. Grundmann, and C. Tropea, "Experimental and computational study of the flow induced by a plasma actuator," Int. J. Heat Fluid Flow **41**, 80 (2013).
[26] R. L. Simpson, "Turbulent boundary-layer separation," Annu. Rev. Fluid Mech. **21**, 205 (1989).
[27] J. A. Vernet, R. Örlü, and P. H. Alfredsson, "Flow separation control behind a cylindrical bump using dielectric-barrier-discharge vortex generator plasma actuators," J. Fluid Mech. **835**, 852 (2017).
[28] A. Seifert, in *Instability and Control of Massively Separated Flows*, edited by V. Theofilis and J. Soria (Springer International Publishing, 2015), pp. 59–64.
[29] T. N. Jukes and K. S. Choi, "Dielectric-barrier-discharge vortex generators: characterisation and optimisation for flow separation control," Exp. Fluids **52**, 329 (2012).
[30] T. N. Jukes and K. S. Choi, "On the formation of streamwise vortices by plasma vortex generators," J. Fluid Mech. **733**, 370 (2013).